International Journal of Microwave and Wireless Technologies

cambridge.org/mrf

High selectivity wideband 180° phase shifters with the functionality of vertical transition

Yu Zhu, Kaijun Song and Yong Fan

EHF Key Laboratory of Science, University of Electronic Science and Technology of China, Chengdu, 611731, China

Research Paper

Cite this article: Zhu Y, Song K, Fan Y (2021). High selectivity wideband 180° phase shifters with the functionality of vertical transition. *International Journal of Microwave and Wireless Technologies* **13**, 240–246. https://doi.org/10.1017/S1759078720001105

Received: 28 April 2020
Revised: 21 July 2020
Accepted: 22 July 2020
First published online: 19 August 2020

Key words:
180° phase shifter (PS); high selectivity; vertical transition (VT); wideband

Author for correspondence:
Kaijun Song,
E-mail: ksong@uestc.edu.cn

Abstract

In this paper, a high selectivity wideband 180° phase shifter (PS) with the functionality of vertical transition is presented. The whole circuit is realized based on the hybrid microstrip/slotline (SL) structure. By introducing the short-circuited microstrip stepped-impedance resonators, two transmission zeros are created to improve the selectivity of the PS. With the SL in the center ground layer, a frequency independent 180° PS can be obtained. The even/odd-mode equivalent circuits of the proposed PS are analyzed to guide the design. Finally, a practical wideband 180° PS with high filtering selectivity is designed and fabricated to verify the design theory.

Introduction

Phase shifters (PSs) are widely used in the modern wireless communication and phased array systems [1–16]. In [3–16], several PSs with different techniques have been proposed, such as PSs based on coupled lines [3–7], PSs using loaded transmission lines or stubs [8–10], PS based on the MEMS technology [11], wideband PS using transversal signal-interference technique [12], and PSs designed with synthesis methods [13–16]. For application in the multilayered microwave-integrated circuits, the components with the feature of microstrip-to-microstrip (MS-to-MS) vertical transition (VT) are always necessary [17–19]. Therefore, PSs with the functionality of MS-to-MS VT are more attractive when used in the multilayered circuits and systems.

This paper proposes a high selectivity wideband 180° PS with the functionality of MS-to-MS VT in a two-layered structure. Compared with previously reported wideband 180° PSs, the proposed design shows wider bandwidth, higher selectivity, and an additional functionality of MS-to-MS VT. Based on the even/odd-mode circuit analysis theory, the simplified circuit models of even/odd-mode circuit can be obtained and a systematic design method of high filtering selectivity response is presented. To confirm the design method and performance of the proposed high selectivity wideband 180° PS, a practical PS operating at 3 GHz is simulated and measured.

Analysis of the PS

The structure of the proposed wideband 180° PS consisting of main and reference branches is shown in Figs 1(a)–1(c), which consists of two-layered substrate and three metal layers. Four $\lambda/4$ (λ is the wavelength) microstrip lines (MLs) and two ML stepped-impedance resonators (SIRs) are placed at the top and bottom layers, respectively, whereas five $\lambda/4$ slotlines (SLs) are etched on the common ground layer. To realize the high-impedance SLs at the two sides of the structure and decrease the radiation losses, four shunt-connected low-impedance SLs with the width of w_{s1} are used to replace two short-circuited high-impedance SLs [20]. The MLs at the top and bottom layers share the same physical dimensions. The difference between reference and main branches is only the direction of ML feedlines at the bottom layer.

For better understanding of phase shifting mechanism in the proposed PS, the evolution of *E*-field in the reference and main branches is depicted in Fig. 2. In Fig. 2, the signals of reference and main branches are fed from port 1 in the same orientation and guided to port 2 in the opposite orientations. According to the cross-view of electrical field distribution shown in Figs 2(a) and 2(b), the input *E*-field is converted from the $-y$ direction to the $+x$ direction in the ML to SL transition and propagates as SL waves until SL to ML transition. In the SL to ML transition, the *E*-field of main (reference) branch is converted from the $+x$ direction to the $-y$ ($+y$) direction. Thus, the *E*-fields at the outputs of reference and main branches propagate in the opposite direction, which amounts to 180° inserted phase. Hence, the feature of frequency independent 180° PS can be obtained by changing the coupled orientation of ML feedlines in the SL to ML transition.

The transmission-line model of the proposed wideband PS is shown in Fig. 3(a) and the four shunt-connected SLs are replaced with two SLs with the impedance of Z_{s1}. The electrical

CAMBRIDGE UNIVERSITY PRESS

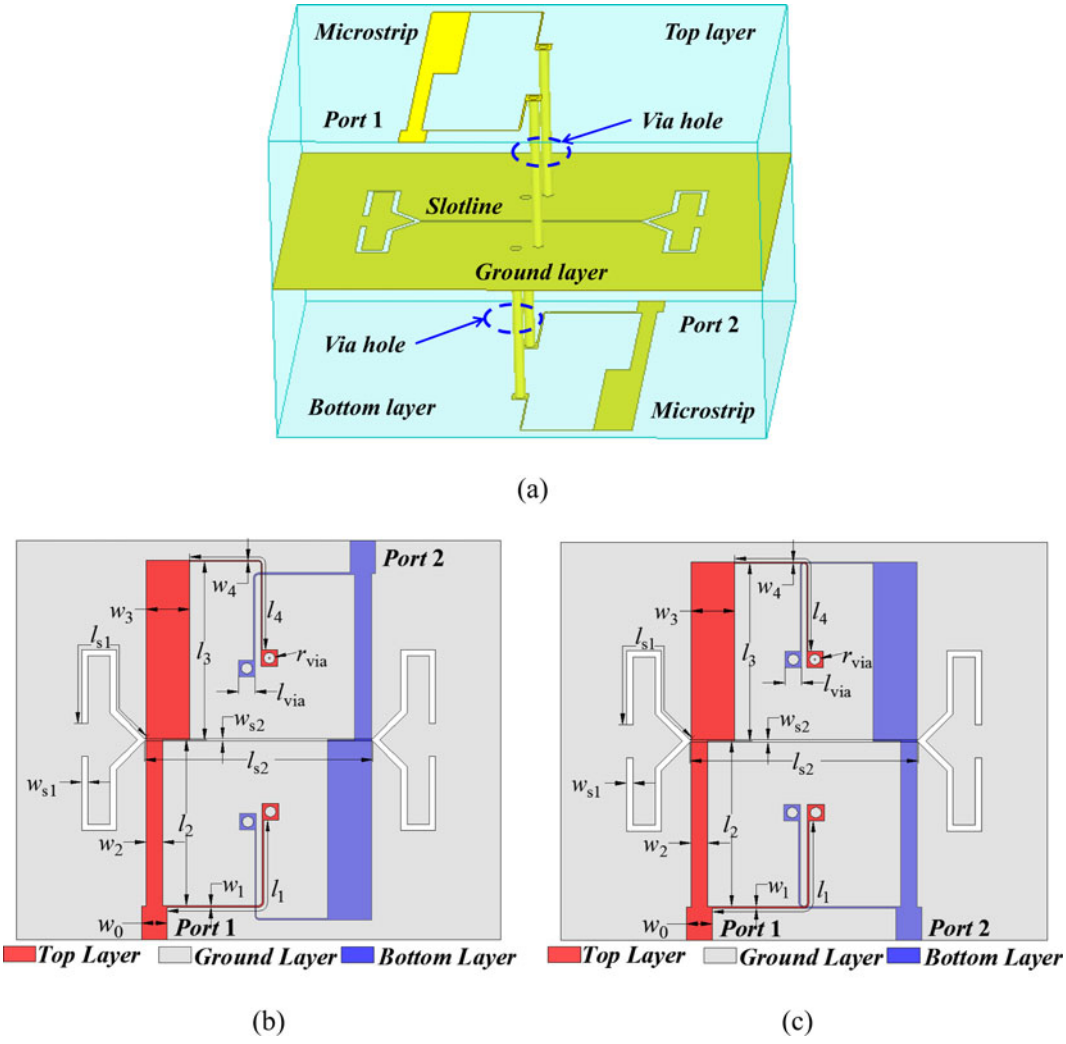

Fig. 1. Structure of the proposed PS: (a) 3D layout of main branch, (b) top view of main branch, and (c) top view of reference branch.

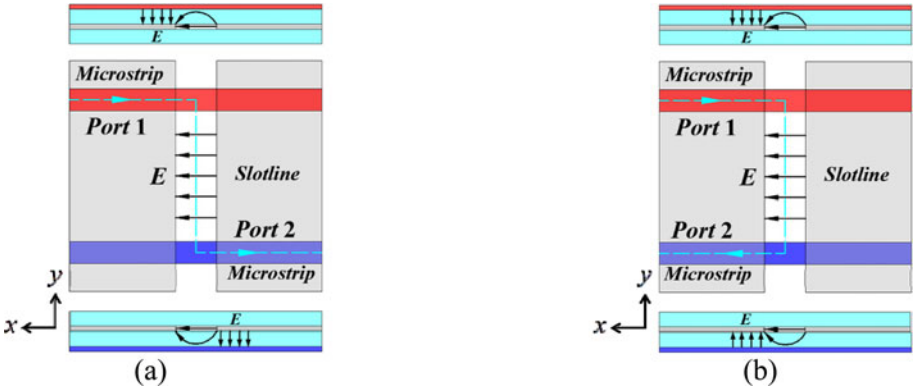

Fig. 2. Evolution of *E*-field: (a) main branch and (b) reference branch (cyan dotted line: signal propagation path; black solid line: *E*-field distribution).

length of the transmission-line section is assumed to be θ (= 90° at the center frequency f_0) and two pairs of impedance transformers with turns ratios of N_1 and N_2 are utilized in this design to equal to discontinuity of MLs and SLs [18].

By absorbing the transformers and normalizing characteristic impedances in Fig. 3(a), even-mode and odd-mode equivalent circuits can be obtained as shown in Figs 3(b) and 3(c), respectively. The relationships between the characteristic impedances of Figs 3(a), 3(b), and 3(c) are shown in Figs 3(b) and 3(c). The odd-mode input impedance can be expressed as

$$z_{ino} = \frac{jz_1z_2(z_{o1}\tan\theta + jz_2\tan^2\theta)}{z_2z_{o1} + jz_2(z_1+z_2)\tan\theta - z_1z_{o1}\tan^2\theta} \quad (1)$$

where

$$z_{o1} = z_{o2} + z_{SIR} \quad (2)$$

https://doi.org/10.1017/S1759078720001105 Published online by Cambridge University Press

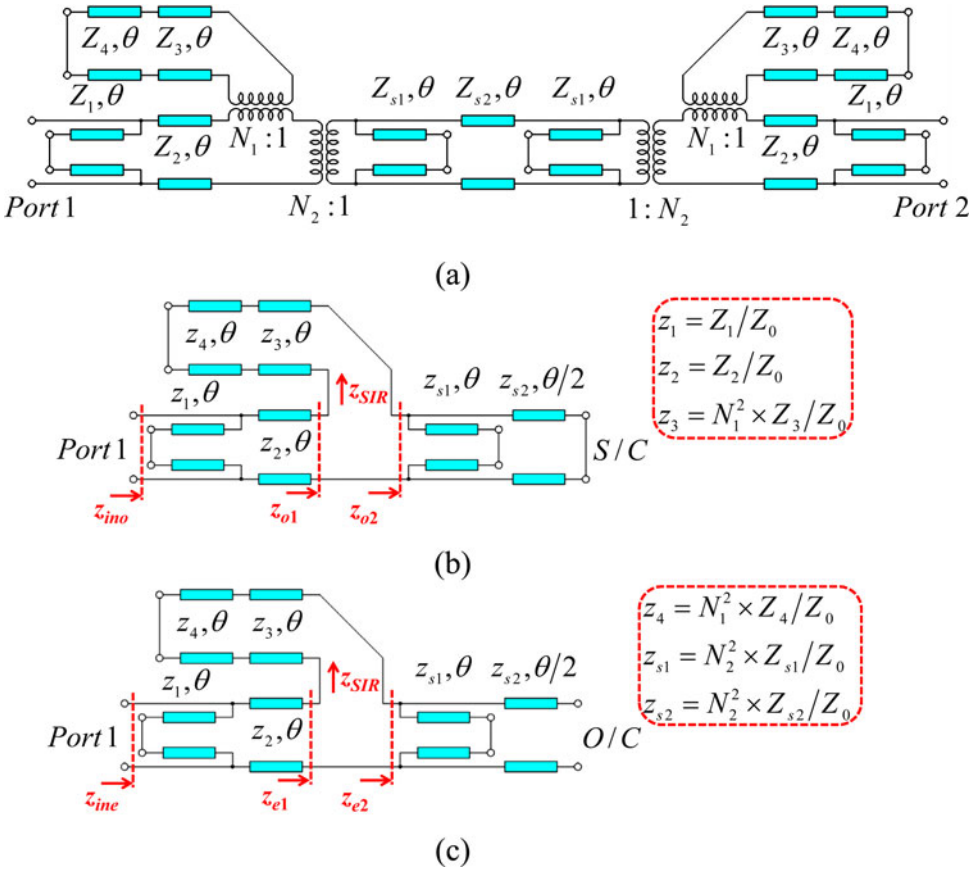

Fig. 3. (a) Transmission-line model of the proposed PS, (b) odd-mode circuit model, and (c) even-mode circuit model.

$$z_{SIR} = jz_3(z_3 + z_4)\tan\theta/(z_3 - z_4\tan^2\theta) \tag{3}$$

$$z_{o2} = jz_{s1}z_{s2}\tan\theta\tan(\theta/2)/(z_{s1}\tan\theta + z_{s2}\tan(\theta/2)) \tag{4}$$

Similarly, the odd-mode input impedance can be obtained as

$$z_{ine} = \frac{jz_1z_2(z_{e1}\tan\theta + jz_2\tan^2\theta)}{z_2z_{e1} + jz_2(z_1 + z_2)\tan\theta - z_1z_{e1}\tan^2\theta} \tag{5}$$

where

$$z_{e1} = z_{e2} + z_{SIR} \tag{6}$$

$$z_{e2} = jz_{s1}z_{s2}\tan\theta/(z_{s2} - z_{s1}\tan\theta\tan(\theta/2)). \tag{7}$$

According to (1)–(7), the *S*-parameters of the proposed filter can be obtained as [21]

$$S_{21} = (z_{ine} - z_{ino})/[(z_{ine} + 1)(z_{ino} + 1)] \tag{8a}$$

$$S_{11} = (z_{ine}z_{ino} - 1)/[(z_{ine} + 1)(z_{ino} + 1)]. \tag{8b}$$

By calculating $S_{21} = 0$, the four transmission zeros (TZs) in the stopband at the frequency range from 0 to $2f_0$ can be obtained as follows:

$$\begin{cases} f_{tz1} = 0; f_{tz2} = (2f_0/\pi)\tan^{-1}\sqrt{z_3/z_4} \\ f_{tz3} = 2f_0;\ f_{tz4} = 2f_0 - (2f_0/\pi)\tan^{-1}\sqrt{z_3/z_4} \end{cases} \tag{9}$$

Based on (9), the positions of the two TZs f_{tz2} and f_{tz4} can be controlled by tuning the ratio z_3/z_4, which is also the impedance ratio of SIR.

According to (8), the characteristic function F can be formulated as [21]

$$F = S_{11}/S_{21} = (z_{ine}z_{ino} - 1)/(z_{ine} - z_{ino}). \tag{10}$$

Figure 4(a) shows the ideal magnitude of *S*-parameters for the proposed PS with a quasi-elliptic equal-ripple response. In Fig. 4(a), the two TZs generated by the SIRs are f_{tz2} and f_{tz4}, the lower cutoff frequency is f_c, and RL is the return loss. The equal-ripple fractional bandwidth (FBW) can be defined as FBW = $2(f_0 - f_c)/f_0$.

In order to design this quasi-elliptic equal-ripple response with desired ripple FBW and RL, the following condition should be satisfied:

$$|F|_{\theta=\theta_0} = |F|_{\theta=\theta_c} = \varepsilon \tag{11}$$

where

$$\theta_0 = \pi/2;\ \ \theta_c = (f_c/f_0)\pi/2;\ \ \varepsilon = 1/\sqrt{10^{RL/10} - 1}. \tag{12}$$

With (11), the RL at f_0 and f_c can be fixed. According to (11), it can be found that:

$$|F|_{\theta=\theta_0} = |(z_{s2}^2 - z_2^4)/2z_2^2z_{s2}| = \varepsilon \tag{13}$$

https://doi.org/10.1017/S1759078720001105 Published online by Cambridge University Press

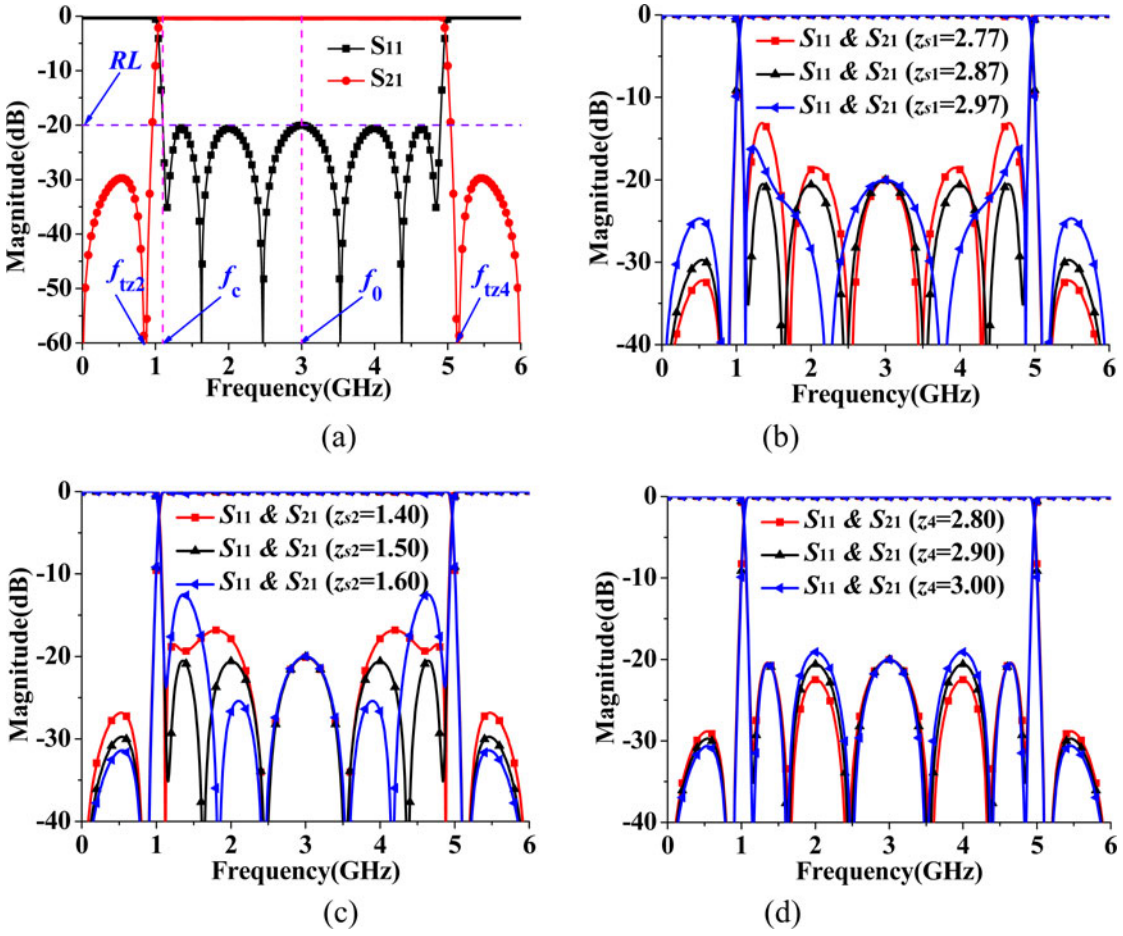

Fig. 4. (a) Ideal *S*-parameters of the proposed PS, (b) *S*-parameters with the variable z_{s1} when $z_{s2} = 1.50$ and $z_4 = 2.90$, (c) *S*-parameters with the variable z_{s2} when $z_{s1} = 2.87$ and $z_4 = 2.90$, and (d) *S*-parameters with the variable z_4 when $z_{s1} = 2.87$ and $z_{s2} = 1.50$.

$$|F|_{\theta=\theta_c} = |(n_0 + n_1 z_1 + n_2 z_1^2)/m z_1^2| = \varepsilon \tag{14}$$

where

$$n_0 = a z_2^2 - z_2^4 \tan^2\theta_c - b z_2^3 \tan\theta_c \tag{15a}$$

$$n_1 = -2(a z_2 + z_2^3)\tan^2\theta_c - b z_2^2 \tan\theta_c (1 - \tan^2\theta_c) \tag{15b}$$

$$n_2 = (a - z_2^4)\tan^4\theta_c + z_2^2(a-1)\tan^2\theta_c - b z_2 (z_2^2 - 1)\tan^3\theta_c \tag{15c}$$

$$m = c z_2^2 \tan^2\theta_c (1 + \tan^2\theta_c) \tag{15d}$$

$$a = z_{o1} z_{e1}|_{\theta=\theta_c} = -[\mathrm{Im}(z_{o1}) \times \mathrm{Im}(z_{e1})]|_{\theta=\theta_c} \tag{15e}$$

$$b = (z_{o1} + z_{e1})|_{\theta=\theta_c}/j = [\mathrm{Im}(z_{o1}) + \mathrm{Im}(z_{e1})]|_{\theta=\theta_c} \tag{15f}$$

$$c = (z_{o1} - z_{e1})|_{\theta=\theta_c}/j = [\mathrm{Im}(z_{o1}) - \mathrm{Im}(z_{e1})]|_{\theta=\theta_c}. \tag{15g}$$

Table 1. List of variables used in Fig. 4

Figure	z_1	z_2	z_3	z_4	z_{s1}	z_{s2}
Fig. 4(b)	1.87	1.17	0.68	2.90	2.77	1.50
	2.24	1.17	0.68		2.87	
	3.59	1.17	0.68		2.97	
Fig. 4(c)	2.84	1.13	0.68	2.90	2.87	1.40
	2.24	1.17	0.68			1.50
	2.00	1.20	0.68			1.60
Fig. 4(d)	2.36	1.17	0.65	2.80	2.87	1.50
	2.24	1.17	0.68	2.90		
	2.13	1.17	0.70	3.00		

By simplifying (13) and (14) with (15), the following formula can be obtained:

$$z_2^4 = \left(1 \pm \sqrt{\varepsilon^4 + 4\varepsilon^2} + 2\varepsilon^2\right) z_{s2}^2 \tag{16}$$

$$(n_2^2 - \varepsilon^2 m^2) z_1^4 + 2 n_1 n_2 z_1^3 + (n_1^2 + 2 n_0 n_2) z_1^2 + 2 n_0 n_1 z_1 = -n_0^2. \tag{17}$$

https://doi.org/10.1017/S1759078720001105 Published online by Cambridge University Press

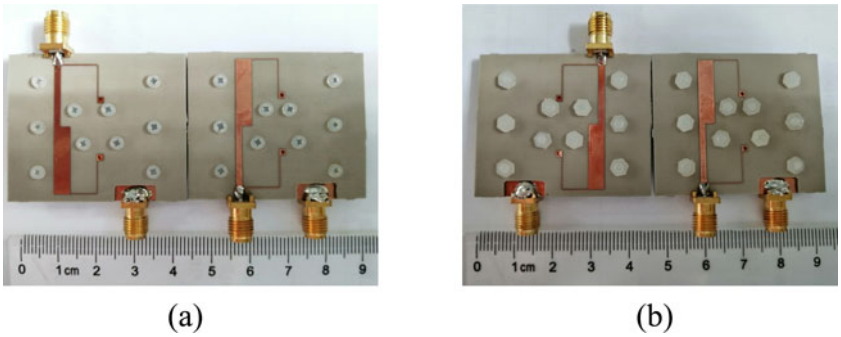

Fig. 5. The photograph of the fabricated circuit: (a) top view and (b) bottom view.

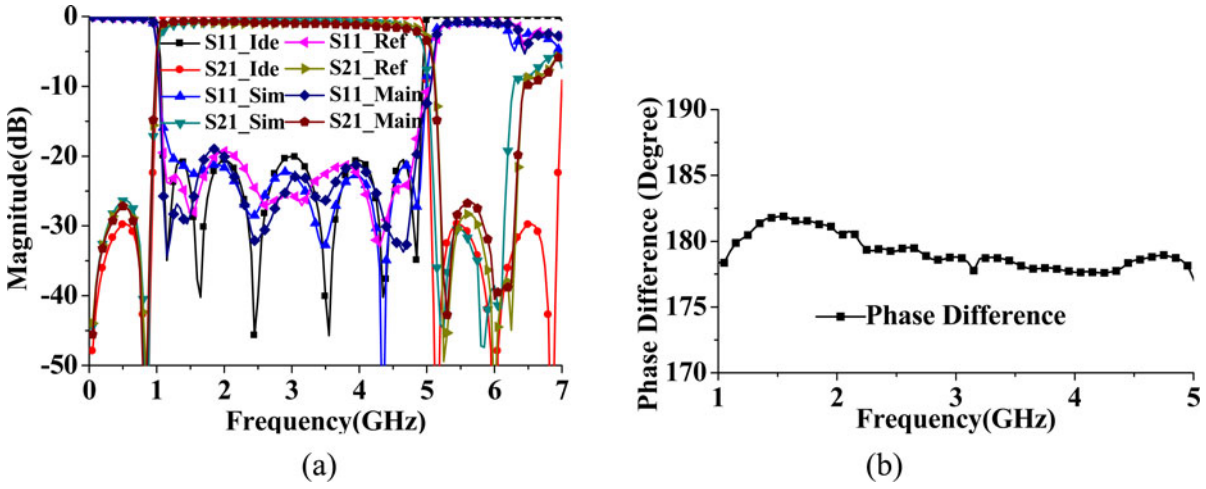

Fig. 6. Simulated and measured results: (a) *S*-parameters and (b) phase difference (Ide: ideal response; Sim: simulated result; Ref: measured result of reference branch; Main: measured result of main branch; optimized dimensions (mm) are summarized as follows: $w_0 = 2.30$, $w_1 = 0.16$, $w_2 = 1.51$, $w_3 = 3.95$, $w_4 = 0.11$, $w_{s1} = 0.56$, $w_{s2} = 0.22$, $l_1 = 16.38$, $l_2 = 15.02$, $l_3 = 16.19$, $l_4 = 14.36$, $l_{s1} = 19.02$, $l_{s2} = 20.63$, $l_{via} = 1.50$ and $r_{via} = 0.50$).

Table 2. Performance comparison with previous wideband PSs

Ref.	IL (dB) at f_0	RL (dB) FBW	PS (°)	TZs	Filtering function	Layers	RC	VT
[4]	0.60	>10 100%	180 ± 8.0	2	No	Single	N/A	No
[7]	1.00	>10 122%	90 ± 5.4	2	No	Single	N/A	No
[12]	1.20	>14 73%	90 ± 5.0	4	Yes	Single	1.43	No
[16]-I	0.90	>11 74%	90 ± 4.5	4	Yes	Single	1.13	No
[16]-II	1.20	>11 51%	90 ± 4.8	4	Yes	Single	1.21	No
This work	**0.99**	**>19 120%**	**180 ± 2.5**	**4**	**Yes**	**Two**	**1.07**	**Yes**

Layers: number of substrate layers; RC: rectangle coefficient (RC = $BW_{20\ dB}/BW_{3\ dB}$, where $BW_{20\ dB}$ is the 20-dB attenuation bandwidth of S_{21} and $BW_{3\ dB}$ is the 3-dB attenuation bandwidth of S_{21}).

With given RL, FBW, f_{tz2} (f_{tz4}), z_{s1}, z_{s2}, and z_4, the values of z_1, z_2, and z_3 can be calculated with (9), (16), and (17). For example, when $f_0 = 3$ GHz, FBW = 127%, and $f_{tz2} = 0.86$ GHz, the responses of *S*-parameters with the variable z_{s1}, z_{s2}, and z_4 are shown in Figs 4(b), 4(c), and 4(d). The list of calculated values of z_1 and z_2 with the variable z_{s1}, z_{s2}, and z_4 in Figs 4(b), 4(c), and 4(d) are shown in Table 1. By tuning the values of z_{s1}, z_{s2}, and z_4, the desirable responses can be obtained.

https://doi.org/10.1017/S1759078720001105 Published online by Cambridge University Press

Based on the above analysis, the values of impedance can be obtained from predetermined f_0, FBW, RL, and TZ f_{tz2} (f_{tz4}). The design procedure for determinant of designed parameters can be given as follows:

(1) Calculate the values of θ_c, ϵ, and z_3/z_4 from predetermined f_0, FBW, RL, TZ f_{tz2} (f_{tz4}) with (9) and (12).
(2) Based on the selected z_{s1}, z_{s2}, and z_4, the values of z_1, z_2, and z_3 can be calculated with θ_c, ϵ, and z_3/z_4 obtained in step (1) and (16)–(17).
(3) Obtain the S-parameters from the calculated values of z_1, z_2, z_3, and selected z_{s1}, z_{s2}, and z_4 in step (2) with (1)–(8).
(4) Tune the values of z_{s1}, z_{s2}, and z_4 and repeat steps (2) and (3) until desirable responses are obtained.

Experimental verification

A practical high selectivity wideband 180° PS operating at 3 GHz with FBW of 127% is designed on a two-layer Arlon AD300C substrate with a permittivity of 2.97 and a thickness of 0.762 mm in each layer. The electric parameters are listed as: $N_1 = 1.06$, $N_2 = 1.08$, $Z_1 = 112.00\ \Omega$, $Z_2 = 58.25\ \Omega$, $Z_3 = 30.17\ \Omega$, $Z_4 = 129.05\ \Omega$, $Z_{s1} = 123.03\ \Omega$, $Z_{s2} = 64.30\ \Omega$, and $Z_0 = 50.00\ \Omega$. The photograph of the proposed wideband 180° PS is shown in Fig. 5. The dimension of the whole circuit is $0.51\lambda_g \times 0.50\lambda_g \times 2$, where λ_g is the guided wavelength at f_0.

The fabricated PS is simulated by the high-frequency structure simulator and measured by the two-port vector network analyzer of Keysight N5244A. The simulated and measured results are plotted in Fig. 6. The measured insertion loss (IL) is 0.99 dB at 3 GHz. The measured bandwidth is 120% from 1.20 to 4.80 GHz for RL higher than 19 dB and phase difference of ±2.5°. Performance comparison between this paper and the-state-of-the-art PS is shown in Table 2. As it can be seen, the designed wideband 180° PS performs well in wider bandwidth, higher selectivity, and an additional functionality of MS-to-MS VT.

Conclusion

In this paper, a high selectivity wideband 180° PS with the functionality of MS-to-MS VT is proposed. With the hybrid microstrip/SL structure, a frequency independent 180° PS can be obtained. Two TZs created by the SIRs are introduced to improve the skirt selectivity of the PS. It can be believed that this high selectivity wideband 180° PS can be used in the wideband radio frequency and microwave systems, which can achieve better performance in the channel selectivity and vertical interconnection.

Acknowledgement. The work was supported in part by the National Natural Science Foundation of China under Grant 61771094 and in part by Sichuan Science and Technology Program under Grant 2019JDRC0008.

References

1. **Eldek AA** (2008) A double rhombus antenna fed by 180° phase shifter for ultrawideband phased array applications. *IEEE Transactions on Antennas and Propagation* **6**, 1566–1572.
2. **Zhou J, Qian HJ and Luo X** (2017) Compact wideband phase shifter using microstrip self-coupled line and broadside-coupled microstrip/CPW for multiphase feed-network. *IEEE Microwave and Wireless Components Letters* **9**, 791–793.
3. **Pu XY, Zheng SY, Liu J, Li Y and Long Y** (2015) Novel multi-way broadband differential phase shifter with uniform reference line using coupled line structure. *IEEE Microwave and Wireless Components Letters* **3**, 166–168.
4. **Guo L, Zhu H and Abbosh A** (2016) Wideband phase shifter with wide phase range using parallel coupled lines and L-shaped networks. *IEEE Microwave and Wireless Components Letters* **8**, 592–594.
5. **Dong Q, Wu Y, Zheng Y, Wang W and Liu Y** (2019) A compact single-layer ultra-wideband phase shifter using weakly coupled lines. *IEEE Access* **7**, 12575–12583.
6. **Yoon H and Min B** (2019) Wideband 180° phase shifter using parallel-coupled three-line. *IEEE Microwave and Wireless Components Letters* **2**, 89–91.
7. **Lyu Y, Zhu L and Cheng C** (2019) A new design of ultrawideband single-layer 90° phase shifter in the view of group delay. *IEEE Microwave and Wireless Components Letters* **6**, 376–378.
8. **Zheng SY, Chan WS and Man KF** (2010) Broadband phase shifter using loaded transmission line. *IEEE Microwave and Wireless Components Letters* **9**, 498–500.
9. **Yeung SH, Mei Z, Sarkar TK and Salazar-Palma M** (2013) Design and testing of a single-layer microstrip ultrawideband 90° differential phase shifter. *IEEE Microwave and Wireless Components Letters* **3**, 122–124.
10. **Yu X, Sun S, Jing X and Zhu L** (2019) Design of ultraflat phase shifters using multiple quarter-wavelength short-ended stubs. *IEEE Microwave and Wireless Components Letters* **4**, 246–248.
11. **Llamas MA, Girbau D, Ribo M, Pradell L, Giacomozzi F and Colpo S** (2011) RF-MEMS uniplanar 180° phase switch based on a multimodal air-bridged CPW cross. *IEEE Transactions on Microwave Theory and Techniques* **7**, 1769–1777.
12. **Zhu H and Guo YJ** (2019) Wideband filtering phase shifter using transversal signal-interference techniques. *IEEE Microwave and Wireless Components Letters* **4**, 252–254.
13. **Lyu Y, Zhu L, Wu Q and Cheng C** (2016) Proposal and synthesis design of wideband phase shifters on multimode resonator. *IEEE Transactions on Microwave Theory and Techniques* **12**, 4211–4221.
14. **Lyu Y, Zhu L and Cheng C** (2017) Single-layer broadband phase shifter using multimode resonator and shunt $\lambda/4$ stubs. *IEEE Transactions on Components, Packaging and Manufacturing Technology* **7**, 1119–1125.
15. **Lyu Y, Zhu L and Cheng C** (2017) Proposal and synthesis design of differential phase shifters with filtering function. *IEEE Transactions on Microwave Theory and Techniques* **8**, 2906–2917.
16. **Lyu Y, Zhu L and Cheng C** (2018) Proposal and synthesis design of wideband filtering differential phase shifters with a pair of out-of-band transmission zeroes. *IEEE Transactions on Microwave Theory and Techniques* **6**, 2828–2841.
17. **Guo X, Zhu L, Wang J and Wu W** (2015) Wideband microstrip-to-microstrip vertical transitions via multiresonant modes in a slotline resonator. *IEEE Transactions on Microwave Theory and Techniques* **6**, 1902–1909.
18. **Yang L, Zhu L, Choi W, Tam K, Zhang R and Wang J** (2017) Wideband microstrip-to-microstrip vertical transition with high filtering selectivity using open-circuited slotline SIR. *IEEE Microwave and Wireless Components Letters* **4**, 329–331.
19. **Yang L, Zhu L, Choi W, Tam K, Zhang R and Wang J** (2018) Wideband balanced-to-unbalanced bandpass filters synthetically designed with Chebyshev filtering response. *IEEE Transactions on Microwave Theory and Techniques* **10**, 4528–4539.
20. **Yang L, Zhu L, Zhang R, Wang J, Choi W, Tam K and Gómez-García R** (2019) Novel multilayered ultra-broadband bandpass filters on high-impedance slotline resonators. *IEEE Transactions on Microwave Theory and Techniques* **1**, 129–139.
21. **Zhu L, Sun S and Li R** (2012) *Microwave Bandpass Filters for Wideband Communications*. New York, NY, USA: Wiley.

https://doi.org/10.1017/S1759078720001105 Published online by Cambridge University Press

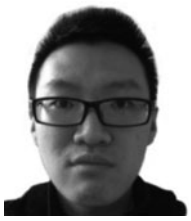

Yu Zhu was born in Anhui, China in 1992. He received his bachelor of engineering degree in electrical information engineering from Southeast University Chengxian College in 2014, and now he is pursuing Ph.D. in electronics science and technology in the University of Electronic Science and Technology of China (UESTC). His current research interests include microwave and RF passive components design.

Kaijun Song (M'09–SM'12) received his M.S. degree in radio physics and his Ph.D. degree in electromagnetic field and microwave technology from the University of Electronic Science and Technology of China (UESTC), Chengdu, China, in 2005 and 2007, respectively. Since 2007, he has been with the EHF Key Laboratory of Science, UESTC, where he is currently a full Professor. From 2007 to 2008, he was a postdoctoral research fellow with the Montana Tech of the University of Montana, Butte, USA. From 2008 to 2010, he was a research fellow with the State Key Laboratory of Millimeter Waves of China, Department of Electronic Engineering, City University of Hong Kong. He has published more than 180 internationally refereed journal papers. His current research fields include microwave and millimeter-wave/THz power-combining technology; UWB circuits and technologies; microwave/millimeter-wave devices, circuits and systems; and microwave remote-sensing technologies.

Yong Fan received his B.E. degree from the Nanjing University of Science and Technology, Nanjing, Jiangsu, China, in 1985, and his M.S. degree from the University of Electronic Science and Technology of China, Chengdu, Sichuan, China, in 1992. He is a senior Member of Chinese Institute of Electronics. From 1985 to 1989, he was interested in microwave-integrated circuits. Since 1989, his research interests include millimeter-wave communication, electromagnetic theory, millimeter-wave technology, and millimeter-wave systems. He has authored or coauthored over 90 papers, 30 of which are searched by SCI and EI.

https://doi.org/10.1017/S1759078720001105 Published online by Cambridge University Press